Spectrochimica Acta Part B: Atomic Spectroscopy 216 (2024) 106930

Contents lists available at ScienceDirect

Spectrochimica Acta Part B: Atomic Spectroscopy

journal homepage: www.elsevier.com/locate/sab

Depth profiling of W—Ta based fusion-relevant samples using picosecond laser ablation

Shweta Soni [a], Sahithya Atikukke [b], Matej Veis [a], Nima Bolouki [c], Pavol Ďurina [a], Pavel Dvořák [c], Martina Mrkvičková [c], Eduard Grigore [d], Pavel Veis [a,*]

[a] Department of Experimental Physics, FMPI, CU, Mlynská dolina F2, 842 48 Bratislava, Slovakia
[b] Department of Astronomy, Physics of the Earth and Meteorology, FMPI, CU, Mlynská dolina F2, 842 48 Bratislava, Slovakia
[c] Department of Plasma Physics and Technology, Faculty of Science, Masaryk University, Kotlarska 2, 611 37 Brno, Czech Republic
[d] NILPRP 409, 077125, Magurele, Bucharest, Romania

ARTICLE INFO

Keywords:
Ps-LIBS
CF-LIBS
Tungsten
WTa(D)
GDOES
Confocal microscopy
Depth profile
Ablation rate

ABSTRACT

This study presents a detailed picosecond LIBS analysis of WTa coatings on Molybdenum substrate with varying layer thicknesses for fusion relevant applications. Ps-LIBS is performed on three WTa layers; two without deuterium (~7 μm thickness) and one with deuterium (~1 μm thickness). The LIBS measurements are conducted under argon gas flow at 5 ± 0.2 mbar pressure with different laser pulse energies (1 mJ, 3 mJ) and 100 spectra are recorded consecutively at one spot on the sample for different set of gate delay/gate width (200/200 ns, 300/300 ns, 450/450 ns). The obtained LIBS and Glow-Discharge Optical Emission Spectroscopy (GDOES) depth profiles are compared with the confocal microscopic measurements showing good agreement. Additionally, the ablation rate and layer thickness are calculated for different experimental conditions. The Calibration-Free LIBS approach is used for elemental analysis and the results are compared with GDOES results. The capability of ps-LIBS to quantify Ta in WTa alloy is explored for 2 at.% of Ta. However, due to higher ablation rate of laser and thin coating in WTaD sample, the layer is irradiated in few laser pulse and therefore, CF-LIBS analysis is not performed for it.

1. Introduction

Nuclear fusion is considered one of the most promising techniques to meet future energy requirements while ensuring a clean energy source [1]. Tungsten (W) and its alloys are currently under active investigation as key candidates for first wall material in divertor or for constructing other plasma-facing components (PFCs) in future fusion devices. Tungsten's exceptional qualities, such as low Tritium retention, a low sputtering rate, high thermal conductivity, low erosion, and robust mechanical properties, make it a prominent and favourable choice for PFC materials [2]. Despite these advantages, the use of bulk tungsten introduces several challenges such as higher electrical conductivity, potentially causing issues with eddy currents [3]. Furthermore, the challenges associated with bulk Tungsten include its hardness, brittleness, and substantial weight, which present difficulties in machining processes. Additionally, the utilization of Tungsten as a high Z material, necessitates the maintenance of a lower plasma impurity content to prevent elevated core radiation losses, distinct from the requirements for low Z wall material a consequent plasma impurities due to the sputtering. To address this limitation, researchers have proposed the use of materials with tungsten coatings for fusion-relevant applications [4]. In *tokamaks*, where the plasma temperature reaches extremely high levels for the initiation of the fusion process and energy production, the neutralization of some Hydrogen ions occurs, leading to power losses in the plasma. To mitigate such issues, the utilization of an effective Hydrogen absorbent material is crucial. Tantalum (Ta), similar to Tungsten, possesses qualities such as higher mechanical strength and resistance against re-crystallization. Moreover, Tantalum is known for its efficient Hydrogen absorption capabilities, making WTa coated fusion relevant materials a promising candidate for applications requiring a good Hydrogen absorbent material for plasma wall interactions in fusion devices [5].

The efficient operation of fusion devices requires the constant monitoring of plasma facing components, first wall and divertor for safety measures and to monitor erosion, impurity deposition and mainly fuel retention [6,7]. These processes are known to affect the *tokamak*

* Corresponding author.
E-mail address: pavel.veis@fmph.uniba.sk (P. Veis).

https://doi.org/10.1016/j.sab.2024.106930
Received 29 February 2024; Received in revised form 22 April 2024; Accepted 23 April 2024
Available online 26 April 2024

operation significantly and shortening the device's lifetime. To avoid this and ensure safe operation of fusion devices, plasma facing components are monitored constantly. There are various diagnostics methods used for such analysis, however other conventional methods such as Secondary Ion Mass Spectrometry (SIMS), Glow-Discharge Optical Emission Spectroscopy (GDOES), X-ray Photo-electron Spectroscopy (XPES), Auger electron spectroscopy, and Energy-dispersive X-ray spectroscopy are mainly offline techniques. Laser based methods are among the best methods to perform such an in-situ analysis in extreme environments.

In the pursuit of effective elemental characterization in these fusion-relevant materials, Laser Induced Breakdown Spectroscopy (LIBS) has emerged as a highly promising analytical tool. Renowned for its versatility and capability for in situ measurements, LIBS holds substantial potential to enhance our understanding of tungsten based materials within the extreme environment of fusion reactors [8]. The advantages of LIBS, including micro-destructiveness, portability, flexibility, and minimum sample pre-treatment, make it a suitable candidate for such applications. Each laser pulse that generates plasma yields one LIBS spectrum, offering detailed information about the coated layer. LIBS offers depth information about the coating, when consecutive spectra are recorded for several laser pulses generating plasma at a specific spot on the target surface [9]. This capability allows for a comprehensive understanding of the composition and characteristics of the material at different depths, contributing to a more thorough analysis of the coated layers in fusion relevant materials.

Nanosecond lasers are commonly employed in LIBS analysis however, their typical duration leads to several challenges; such as thermal effect and matrix effect [10,11]. In LIBS due to the strong coupling of the continuum with molten material at the target surface, matrix effect is prominent in LIBS spectra. Furthermore, thermal effects modify density profiles, hindering precise measurements in depth profiling analysis. These combined characteristics collectively reduce the accuracy of LIBS, especially for light elements, under these conditions [12]. The shot-to-shot LIBS reproducibility is poor due to the complex processes involved in laser-induced plasma. Previous studies in laser ablation have demonstrated that employing short pulses leads to a reduction in material deposition around the ablation area. Furthermore, these short pulses have been shown to significantly enhance the reproducibility of material ablation [13]. For laser pulses with short pulse duration (in order of tens of picosecond or less), the thermal diffusion length being smaller than the laser spot results in minimal melting and improved reproducibility of ablation, primarily attributed to the direct transition of material to the vapor or plasma phase without undergoing melting [14,15]. In contrast to nanosecond laser ablation where melted material forms in the ablation region, and the ablated material is predominantly ionized by electron-ion collisions, ps laser-induced plasma is generated through the direct photoionization of the material via a multi-photon process [15,16]. Given the advantages of ps-LIBS, A. Bultel et al. have reported the use of ps-LIBS for W/Al based fusion relevant material analysis and a comparative study of ns-LIBS and ps-LIBS is discussed by A. M. Roldan et al. [17–21].

This study suggests employing ps-LIBS analysis for fusion-relevant samples with WTa and WTa + D coatings on Mo substrates. The research focuses primarily on elemental quantification and depth analysis of WTa deposited samples on the Mo substrate with Ta content 2-10 at.%. Additionally, we conducted a similar analysis for samples with the incorporation of deuterium in the deposited layer (WTaD/Mo), characterized by an additive composition of deuterium in the deposited layer. The study demonstrates LIBS emission spectrum from the WTa/Mo sample, and a detailed discussion on the depth analysis of the crater and the layer, building upon the findings of our earlier studies [22]. The depth profiling results are compared with the results from GDOES method which is basically an OES technique that uses a glow discharge to sputter material from the surface of a sample. This sputtered material is then atomized, excited, and subsequently emits characteristic radiation, allowing for the determination of elemental composition and depth profiling analysis. Additionally, the investigation incorporates a detailed crater analysis using 3D scanning confocal microscopy (Keyence VK-X3000), offering valuable insights on ablation rates and the thickness of the coated layer. Furthermore, Calibration-free LIBS approach is adopted for elemental quantification in the thin coatings [23,24]. Plasma parameters, specifically electron temperature (T_e) and electron density (n_e), are evaluated using multi elemental Boltzmann plot (MEBP) method and from the H_α line (656.28 nm) broadening, respectively. In addition to it, one of the objective of this work is to determine the thickness of the coated layer, which can be realised by plotting depth profile, followed by subsequent establishment of the elemental composition of the layer using CF-LIBS. The obtained LIBS results are then compared with GDOES method, showing a significant agreement between the observations of the two techniques.

2. Materials and methodology

2.1. Material

LIBS analysis is conducted on three sample, namely EU2–72, EU2–73, and EU2–75. Samples EU2–72, and EU2–73 has coating of W and Ta deposited onto Mo substrates, while the sample EU2–75 contains thin coating of W, Ta and D deposition. The composition of deposited layers are tabulated in Table 1. The samples are in the form of 1 mm thin square metallic pieces with dimensions of $12mm \times 12mm$. The WTa coatings are prepared with magnetron sputtering process while the WTa+D coating are prepared with high power impulse magnetron sputtering (HiPIMS) inside the vacuum chamber which is kept under deuterium afterglow discharge atmosphere during the sputtering process. The thickness of thin layers are measured with GDOES technique with 6.68 μm, 6.99 μm and 1.09 μm for samples EU2–72, EU2–73 and EU2–75 respectively. To measure the thickness of a coating using the GDOES method, the elemental chemical composition is monitored over time as the glow discharge sputters material from the sample surface. The WinGDOES software program, version 4.2, is utilized for the time/depth conversion of the sputtering process. Relative sputtering rates for different elements (e.g., RW, RMo, RTa, RD) compared to a reference element (RFe) are introduced into the software, based on values obtained from reference literature [25]. As the sputtering progresses, the depth of the sputtered material is periodically checked using an optical microscope with a resolution of 0.2 μm. The depth measurements obtained from the GDOES system are then validated by comparing them with the measurements from the optical microscope. Typically, the agreement between the two methods falls within the range of ±0.5 μm, ensuring accuracy in the determination of coating thickness.

2.2. Experimental scheme

A detailed ps-LIBS experimental scheme is illustrated in Fig. 1. The experiments are performed within a chamber evacuated at 5 ± 0.2 mbar to obtain the LIBS spectra under low pressure. The experimental setup involves a picosecond pulsed laser beam with a pulse duration of 29 ± 4 ps, beam diameter of 4 mm for the laser ablation and plasma creation. The laser beam is focused onto the WTaD sample, securely mounted on the sample holder within the ISO-air-sealed chamber. This focusing is

Table 1
Elemental compositional details of WTa coated samples used.

Sample Index		Substrate	GDOES Layer Thickness (μm)	Layer Composition (*at.*%)		
				W	Ta	D
1	EU2–72	Mo	6,68	90.20	9,80	–
2	EU2–73	Mo	6,99	97.48	2.52	–
3	EU2–75	Mo	1,09	83	7	10

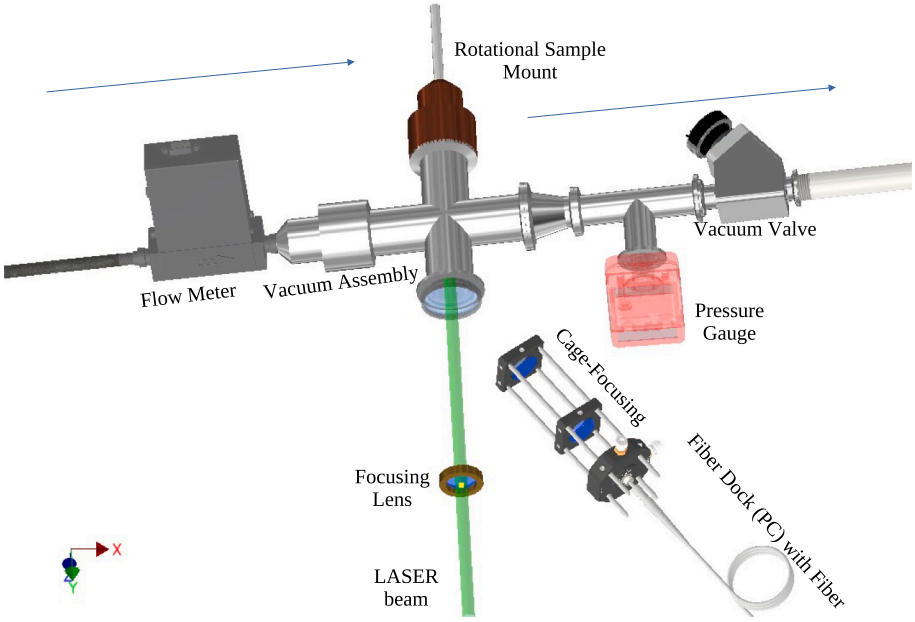

Fig. 1. Simplified 3D schematic illustrating ps-LIBS within a chamber under argon flow at 5 ± 0.2 mbar pressure. A plano-convex lens (f = 125 mm) focuses the laser beam onto a WTa/Mo sample. Pressure and gas flow are regulated using a mass flow-meter. Plasma emission is collected by a cage-based optical system of two plano-convex lenses, coupled to an optical fiber followed by the analyses using a spectrometer.

achieved using a convex lens with a focal length of 125 mm resulting in beam spot diameter of 21.2 μm and fluence of 6.16 J/cm^2 and 45.08 J/cm^2 corresponding to 1 mJ and 3 mJ of laser energies. The Nd: YAG laser is operating at second harmonics; 532 nm. The experimental chamber is a aluminium based four-way cross-like chamber with each side of 40 mm in diameter. The front arm is customarily designed and cut shorter to have better access for plasma collection. This front arm is equipped with a quartz window, serving the purpose of focusing the laser beam onto the sample and also enabling the collection of LIBS signals from outside the chamber. The sample holder is securely fixed to the opposite end of front arm, and offers the added advantage of a spiral rotation, allowing to have a fresh spot on the sample for LIBS measurements. The whole setup is mounted on linear transnational mount, giving it an addition direction of sample movement and enhancing its capability for experimental flexibility. One of the side arms is attached with a reducing nipple, transitioning from 40 mm to 25 mm. The pressure inside the chamber is monitored with the pressure gauge (Pfeiffer, TPG - 201) connected to it. A *'tee'* is connected to a pressure valve (VAT, S265), giving an access to control the flow of the gas inside by further attaching it to a pump. The opposite side arm of the chamber is connected to a custom-made reducing unit, transitioning from 40 mm to 20 mm, featuring a clamp on the smaller end. This unit is then linked to a standard mass flow meter (Omega, FMA - 2601 A) which controls the technical argon gas flow with the purity of 99.996%. The flow of argon is set to 150 sccm to maintain the pressure inside the chamber at 5 ± 0.2 mbar.

The LIBS experimental involves ignition of plasma by laser irradiation, followed by the collection of plasma emission and analyses of emission spectra by echelle spectrometer (Mechelle 5000, 200 – 850 nm) equipped with an ICCD detector (iStarDH743, AndorTech). The emission from plasma is collected using a cage based telescopic system with a pair of two plano-convex lenses with focal lengths of 175 mm and 50 mm. The collected signal is then transported to the spectrometer via a standard UV-VIS fiber optic cable. For spectrometer calibration, an HgAr lamp is employed to calibrate the echellogram position across the entire spectral range of the spectrometer (200 – 850 nm). Additionally, for sensitivity calibration, we followed the methodology outlined in our previous paper [26]. The sensitivity curve was assessed independently in the VIS – NIR range using a W lamp and the grey body continuum spectrum simulation. In the UV range, calibration was conducted utilizing the molecular bands branching ratio with the NO (A-X) and N_2 (C-A) transitions. The experiment is performed at three different observation windows of gate delay and gate width; 200 ns – 200 ns, 300 *ns* – 300 ns, and 450 *ns* – 450 ns and at two different laser energies; 1 mJ and 3 mJ. These experimental parameters are optimized for the CF-LIBS analysis Two sets of 50 laser pulses are recorded at each spot to have a total of 100 laser shots for depth profile analysis. The experimental setup facilitates a regulated gas flow and maintain pressure parameters to ensure a precisely defined experimental environment for air-sealed analysis, effectively preventing interference from atmospheric hydrogen.

3. Results and discussions

3.1. LIBS spectral response from WTa coated sample

Various atomic and ionic lines of W, Ta and Mo I are observed in the LIBS spectra recorded across the wavelength range of 200 – 850 nm. The spectra illustrated in Fig. 2 shows the LIBS emission spectra from the sample EU2–72 at different laser shots at various depth under the argon gas flow at 5 ± 0.2 mbar. The spectra represents W I, Ta I and Mo I lines in the spectral range 518 – 566 nm. The spectra is recorded as two consecutive sets of 50 laser shots concluding 100 laser shots at each spots. The data is further consolidated to derive average from multiple laser shots (to be precise, signal from the deposited layer) for better resolution. It required about 20 laser shots to penetrate through the coating in EU2–72 at 3 mJ laser pulse energy while in case of 1 mJ, the number of laser pulses required to cross the layer is 100. Fig. 2 comprises 8 sets of spectra, plotted against the wavelength across multiple laser shots which represents the average spectra from five consecutive laser shots along the z-axis laser shots. In Fig. 2, first four spectra are averaged ±2 shots while the spectra 5 and 6 are averaged ±5 laser shots and the last two are averaged by ±15. The averaging of spectra allows to enhance the signal to background ratio. The spectra demonstrates the presence of W I lines at 522.29 nm and 551.47 nm Ta I lines at 535.31 nm and 564.5 nm. Initially W I line at 522.29 nm appears to decrease as the number of laser shots increases and evidently persists due to the

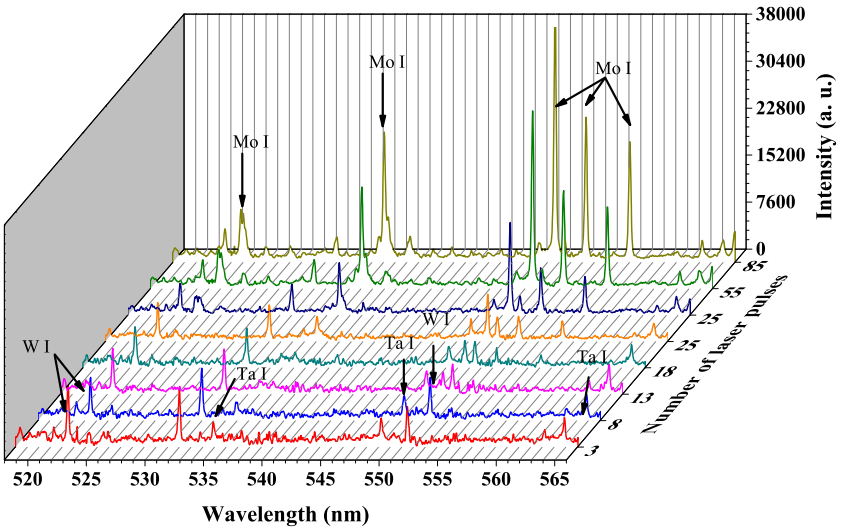

Fig. 2. Evolution of LIBS emission spectra from EU2–72 sample across multiple laser shots within the spectral range 518–566 nm, highlighting presence of W I and Ta I lines in first few spectra and later emergent of Mo I lines when laser penetrates the coating and hits the substrate after 20 laser shots at 3 mJ laser energy. Each data point on represents the average spectra from a selected number of laser shots along the z-axis.

emergence of Mo I line at 523.8 nm as we approach the substrate. While Ta lines disappears as the laser penetrates the deposited coating and Mo I lines clearly emerges after 20 laser shots. Prominent Mo I lines are observed at 550.66 nm, 553.26 nm, and 557.03 nm. The Ta lines are comparatively weak due to its low concentration in the sample and therefore, spectral lines are selected carefully to avoid inaccuracies in the quantification due to self-absorption, and spectral interference primarily.

3.2. Crater analysis with confocal microscopy

In our study, we have applied 3D laser scanning confocal microscope (VK-X3050, Keyence), for analyzing the craters formed during LIBS measurements. This microscopic technique provides depth measurements along the vertical axis (z-axis). For the laser confocal mode we utilized, the accuracy in the vertical direction is typically below 0.2 μm. Additionally, the repeatability in this direction is specified to be below 0.1 μm for the 10× objective lens, which is used in this work. The craters are formed as a result of 100 consecutive laser pulses focused on sample

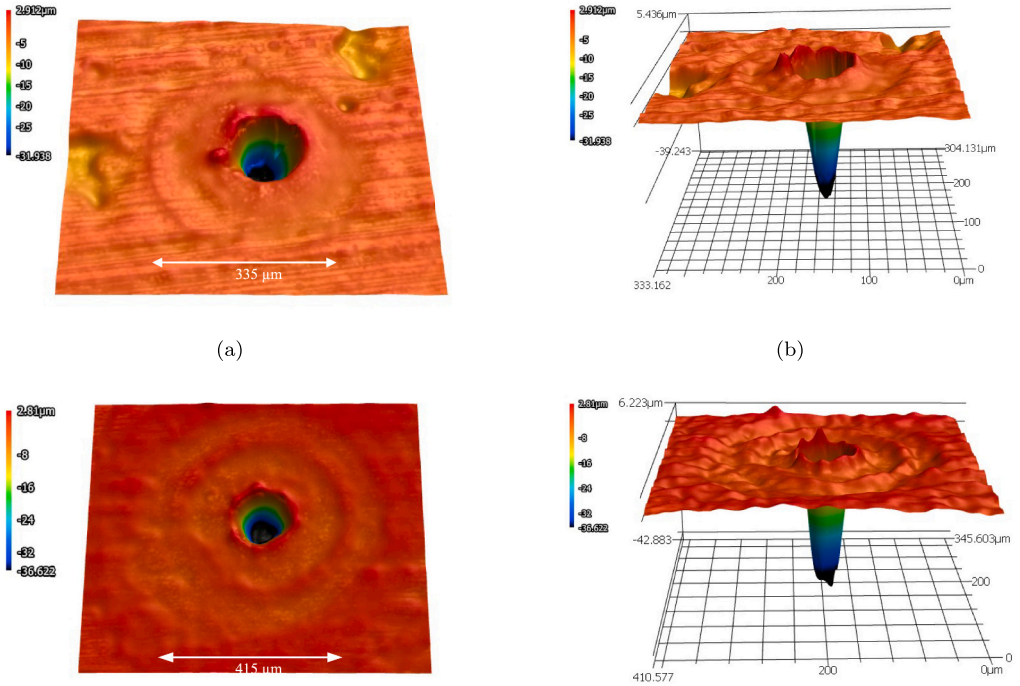

Fig. 3. Confocal microscopic images of the crater created by ps-LIBS corresponding to 100 laser pulses. 2D image (a) and 3D image (b) of the crater from sample EU2–72 with WTa coating with 6.68 μm thickness. 2D image (c) and 3D image (d) of the crater from sample EU2–75 with WTa + D coating with 1.09 μm thickness.

target. Fig. 3a, b, represents the 2D crater image from the samples EU2–72 and its corresponding 3D mapping respectively. Whereas Fig. 3c, d, represents the crater image from the samples EU2–75 and corresponding 3D mapping respectively. The 3D images shows the gradual reduction in the depth diameter indicating that after a number of laser pulses the depth profile saturates. Through this technique, we have evaluated the ablation rate, depth of crater and thickness of layer. For EU2–72, the crater depths for laser energies of 1 mJ and 3 mJ are measured at 13.34 μm and 28.92 μm, respectively. The estimated ablation rates for EU2–72 are 0.133 μm/pulse and 0.28 μm/pulse for 1 mJ and 3 mJ laser pulses, respectively. Additionally, the estimated thickness of the ablated layer for EU2–72 is 7.35 μm and 8.20 μm for 1 mJ and 3 mJ laser energies, respectively. Similarly, for EU2–73, the crater depths for 1 mJ and 3 mJ laser energies are measured at 13.15 μm and 17.82 μm, respectively. The ablation rates are calculated as 0.131 μm/pulse and 0.178 μm/pulse for 1 mJ and 3 mJ laser pulses, respectively. The estimated thickness of the ablated layer for EU2–73 is 6.68 μm and 4.79 μm for 1 mJ and 3 mJ laser energies, respectively. The ablation rate is lower for 1 mJ laser energy while the thickness values are closer to what measured by GDOES method however, in case of 3 mJ laser energy the error in thickness measurement of coating is higher.

3.3. Depth profiling of WTa-based coating

The study also presents a comprehensive depth profile of WTa coated samples; EU2–72 and EU2–72 from glow discharge emission spectroscopy (GDOES). The depth profiles are constructed from atomic lines of W, Ta, Ti, and Mo and illustrated in Fig. 4a, b and c. All the samples are prepared through magnetron sputtering deposition. During the sample preparation of EU2–72 and EU2–73 with magnetron sputtering, two types of substrates are used simultaneously; Ti and Mo for preparation of WTa coating, where Ti is taken as a reference substrate. In the GDOES depth profile of EU2–72 and EU2–73 are performed on WTa coating on the Ti substrate samples and shows the decrease in the W/Ta graph and at the interface both W and Ti line intersect each other. While depositing WTaD on the substrate (EU2–75), an additional D-atom source (D_2 glow discharge) was added in the setup during the magnetron sputtering process. Fig. 4a, b illustrates that tungsten concentration begins to drop at 6.00 μm and almost immediate rise in Ti concentration. While Ta can be observed declining shortly after tungsten, by by a fraction of μm. The concentration of W and Ti are observed to be same at the interface of the coating and the substrate at around 6.68 μm for EU2–72 and 6.99 μm for EU2–73. For deuterium containing sample, the depth profiling of D_α line (656.09 nm) in LIBS becomes very difficult due to the dominating presence of H_α line at 656.28 nm. Fig. 4c shows the GDOES depth profile for WTaD coated sample named EU2–75 sample. It is evident from Fig. 4d that the depth of the sample is 1.09 μm however D and Ta profile start descending around 0.9 μm which also shows the non-uniform distribution of these elements across the sample thickness. Fig. 4d illustrates the behaviour of the Mo I line at 550.67 nm, with the black curve representing EU2–72 and the red curve representing EU2–73, both obtained at a laser energy of 3 mJ. This graph showcases the intensity variation of the Mo I spectral line as laser pulses are applied to a small spot on the target. Such variation offers valuable compositional insights

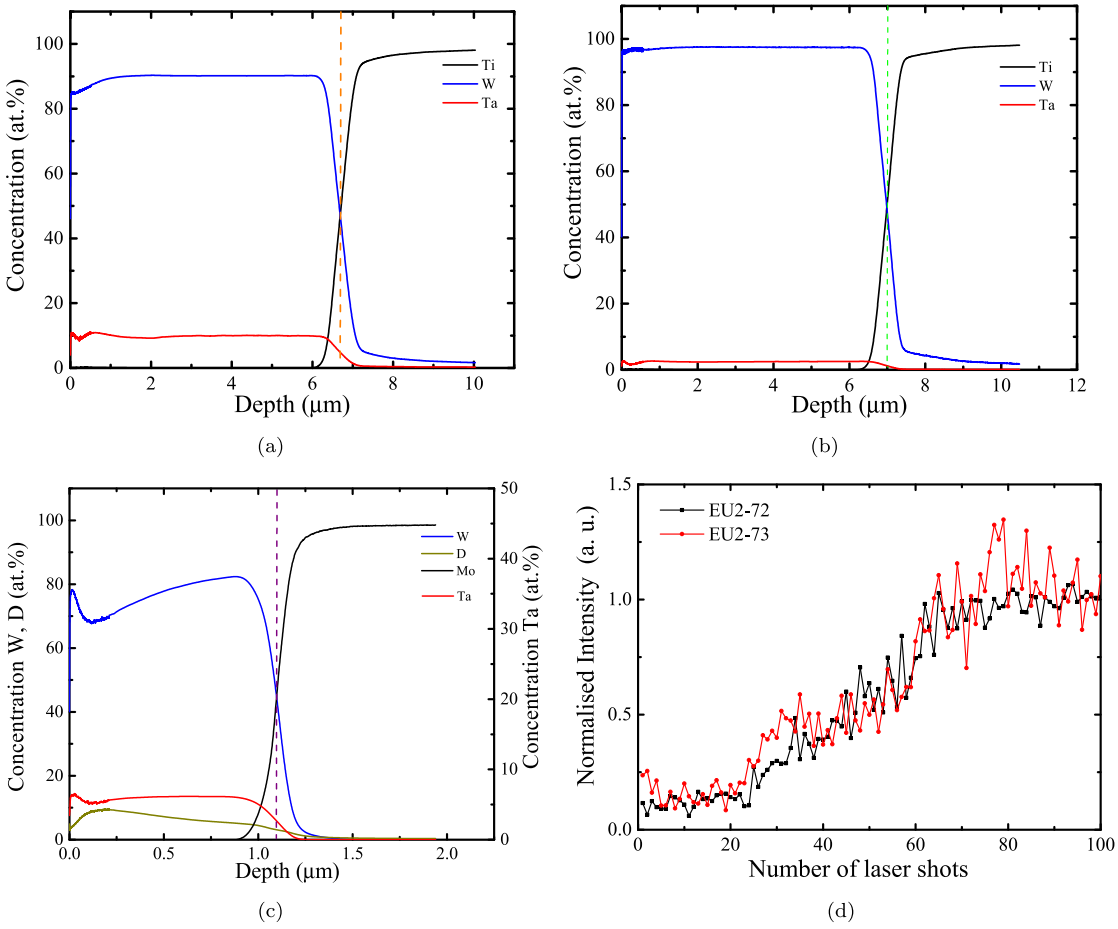

Fig. 4. (a) GDOES depth profile of sample EU2–72 showing the layer thickness 6.68 μm; (b) GDOES depth profile of sample EU2–73 showing the layer thickness 6.99 μm; (c) GDOES depth profile of sample EU2–75 showing the layer thickness 1.09 μm; (d) Variation of Mo I line intensity (550.67 nm) at different depth of craters with the number of laser shots (representing the depth of the layer).

into the sample's depth. With the prior knowledge of the ablation rate acquired from scanning confocal microscopy, the depth of the layer can be accurately evaluated.

3.4. Plasma parameter evaluation and CF - LIBS analysis

The compositional quantification of individual layers in the samples is evaluated utilizing the CF-LIBS approach. The method was introduced by Ciucci et al. [23] and recently well explained in a review paper by Hu et al. [24]. CF-LIBS has evolved into a well-established technique within the field of nuclear fusion for determining the elemental composition of first-wall materials, including D/T fuel retention, as evidenced by [7,27]. The LIBS plasma is non-homogeneous and transient, requiring optimized temporal and spatial parameters to meet the necessary condition of local thermodynamic equilibrium (LTE), which is checked by McWhirter's criterion given in eq. (1).

$$n_e > 1.6 \times 10^{12} T^{1/2} (\Delta E)^3 \tag{1}$$

In addition to meeting LTE condition, plasma must also be created through stoichiometric ablation and must be optically thin, meaning the influence of self-absorption (SA) in the selected lines for CF-LIBS quantification should be negligible. In order to select SA-free lines from all W I-II and Ta I-II lines, the SA probability of spectral lines are assessed by multiplying the transition probability A_{mn} by the relative population of the absorbing state. This is calculated according to the Boltzmann distribution with a characteristic estimated temperature of $\sim 0.5\ eV$ for the outer plasma layer as discussed in our previous work reported by M. Horňáčková et al. [28]

For spectral analysis with CF-LIBS, the evaluation of plasma parameters such as electron temperature and electron density is essential. Once the LTE condition is established, the population of plasma species in energy states can be derived from Boltzmann distribution and the electron density is evaluated by evaluating the full width half maxima of H_α spectral line at 656.28 nm using following Eq. [29];

$$\lambda_{1/2} = \frac{n_e}{10^{16}} w \tag{2}$$

where $\lambda_{1/2}$ is the full width of half area of H_α line, n_e is the electron density while w is the stark broadening parameter available in literature. The estimated temperature evaluated using Boltzmann plot is the excitation temperature which is equivalent to the electron temperature (T_e) under the LTE condition where all the process are balanced by principle of detailed balancing i.e. neutrals, ions, electrons and photons in plasma have same temperature. The electron temperature determined by Boltzmann plot is evaluated from eq. (3) given below:

$$ln\frac{I_{mn}\lambda_{mn}}{A_{mn}g_m} = -\frac{E_m}{K_B T} + ln\frac{FC_x}{U_x(T)} \tag{3}$$

where, F represents the experimental parameter that encompasses both the efficiency of the collection system and the density of the plasma.C_x is the concentration of the element x. While A_{mn} is the Einstein coefficient corresponding to the transition mn and signifies the spontaneous transition probability. g_m, and E_m represent the statistical weight and energy of the upper level m, respectively, while $U_x(T)$ stands for the partition function at temperature T. Eq. (3) can be expressed into a linear expression as;

$$y = mx + q_x \tag{4}$$

with the following expressions for y, x, m and q_x;

$$y = ln\frac{I_{mn}\lambda_{mn}}{A_{mn}g_m} \tag{5}$$

$$x = E_m \tag{6}$$

$$m = -\frac{1}{K_B T} \tag{7}$$

$$q_x = ln\frac{FC_x}{U_x(T)} \tag{8}$$

A linear relationship between E_m and $ln\left(\frac{I_{mn}\lambda_{mn}}{A_{mn}g_m}\right)$ can be achieved through linear regression, yielding what is commonly referred to as a Boltzmann plot. This plot can be individually drawn for each type of atom and ion. By analyzing the slope (m) and intercept (q_x) of the line, which correspond to Eqs. 7, and 8, respectively, the plasma temperature and concentration of specie x can be deduced.

In this study initially, the electron temperature is deduced from the Boltzmann plot of W I-II and Ta I-II, yielding values that are notably close, as demonstrated in Figs. 5a and 6a. To achieve more precise values of (T_e), we transformed the Boltzmann plot (BP) into a multi-elemental BP by adjusting the y - values with the corresponding center of mass for each species, as illustrated in Figs. 5b and 6b. This correction further enhanced the accuracy of the analysis by providing more precise electron temperature. The Boltzmann plots for the sample EU2–72, and EU2–73 are presented in Figs. 5a, 6a respectively. Each figure showcases the Boltzmann plots obtained from W I-II and Ta I-II lines extracted from the LIBS emission spectra of the WTa layer without D. The measurements are performed with ps Nd:YAG laser operating at its second harmonics with a pulse duration of 29 ± 4 ps and 3 mJ laser energy and at low pressure at 5 ± 0.2 mbar. The different sets of gate delays and gate width are used; 200 ns - 200 ns, 300 ns - 300 ns and 450 ns - 450 ns with two consecutive sets of kinetic series measurement of 50 laser pulse at each spot on the sample surface. The spectral transitions and corresponding parameters necessary for constructing the Boltzmann plot are evaluated utilizing standard databases such as the NIST database and the Kurucz database [30,31]. The estimated electron temperatures for these sets of measurements parameters are tabulated in the Table 2. Due to the quick expansion of plasma at low pressure at 5 ± 0.2 mbar ($\sim$ 200 times lower pressure than atmosphere), leads to the typically low T_e value [32]. The data points plotted on Boltzmann plots represent averages obtained from 20 laser pulses emitted from the layer only. This averaging process serves to enhance the spectral response by reducing noise, ensuring a sufficiently intense and reliable signal for analysis from WTa layers. Quantifying deuterium (D) in sample EU2–75 using CF-LIBS proves challenging due to the presence of D lines solely in the first initial laser shot, which is insufficient for accurate quantification. This limitation may arise from higher ablation rate of D containing samples (from Confocal Microscopy measurements) and presence of thinner layer of WTaD samples. Optimization of collection optics through various angles to the plasma could enhance detection capabilities.

The electron density (n_e) is determined by analyzing the Stark broadening of the H_α spectral line, as described in reference [29]. The presence of hydrogen could be originated from the gas hose itself, given its technical gas nature with a purity of 99.996%. The evaluation of plasma parameter (T_e and n_e) leads the path to CF-LIBS quantification which are tabulated in Table 2. Table 2 represents the estimated values of plasma parameters (T_e and n_e) for all three sets of gate delay and gate widths; 200 ns - 200 ns, 300 ns - 300 ns, 450 ns - 450 ns at two different laser energies 1 mJ and 3 mJ. The quantification results obtained through CF-LIBS are compared with the concentrations measured using GDOES, including the calculation of relative percentage errors. The quantification error is higher for Ta; $\sim$ 12–40% and for W is as low as $\sim$2% which is comprehensible as W concentration is $\sim$10 times higher than Ta concentration. This discrepancy represents a limitation of the CF-LIBS approach, where higher errors are encountered when analyzing elements present in lower concentrations. It is worth noting that the precision and accuracy achieved in determining plasma parameters significantly influence the reliability of the elemental quantification results. The presented methodology ensures a thorough analysis of the

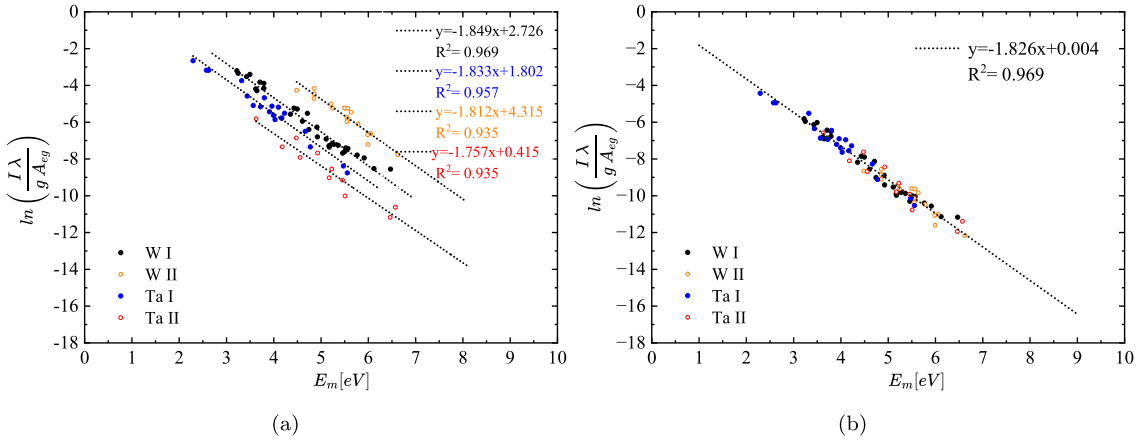

Fig. 5. Boltzmann plots (a) and corresponding multi-elemental Boltzmann plot (b) obtained from W I-II and Ta I-II lines of WTa/Mo (EU2–72 sample) LIBS spectrum (Ar gas, 5 ± 0.2 mbar pressure, ps Nd:YAG laser, 2nd harmonic at 532 nm, pulse duration 29 ± 4 ps and energy 3 mJ, delay 200 ns and gate time 200 ns, spectrum average over first 20 shots corresponding to the layer thickness).

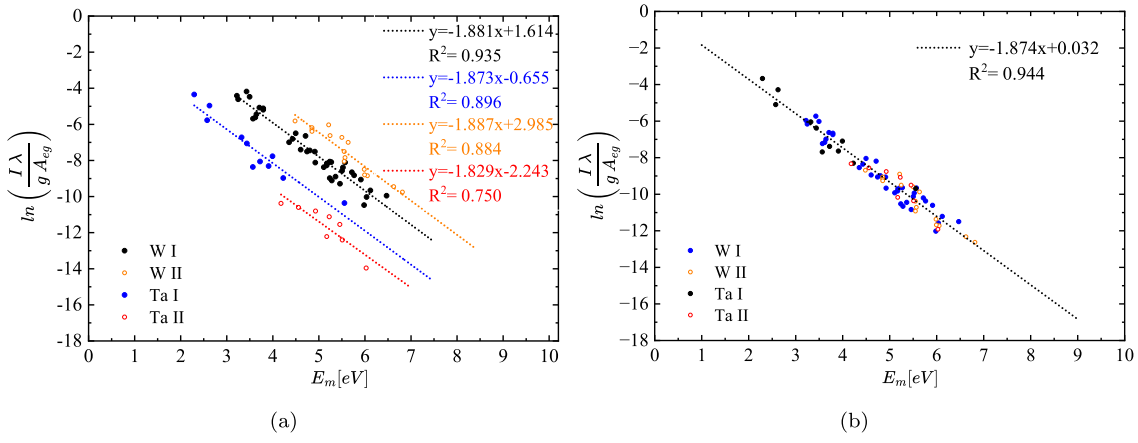

Fig. 6. Boltzmann plots (a) and corresponding multi elemental Boltzmann plot (b) obtained from W I-II and Ta I-II lines of WTa/Mo (EU2–73 sample) LIBS spectrum (Ar gas, 5 mbar pressure, ps Nd:YAG laser, 2nd harmonic at 532 nm, pulse duration 29 ± 4 ps and energy 1 mJ, delay 200 ns and gate time 200 ns, spectrum average over first 100 shots corresponding to the layer thickness).

Table 2
Plasma parameters and Caliberation free LIBS quantification.

Sample	Laser Energy (mJ)	Gate Delay (ns)	T_e (eV)	n_e ($\frac{10^{16}}{cm^3}$)	GDOES conc. (at. %)		CF-LIBS conc. (at. %)		CF-LIBS anl. Error (%)	
					W	Ta	W	Ta	W	Ta
EU2–72	1	200	0.53 ± 0.05	1.79	90.20	9.80	89.87	10.13	2.20	20.21
		300	0.54 ± 0.05	1.46			89.61	10.39	2.53	21.81
		450	0.50 ± 0.08	0.69			89.68	10.32	4.80	40.96
	3	200	0.55 ± 0.04	1.69			89.87	10.13	1.43	12.74
		300	0.54 ± 0.04	2.35			89.61	10.39	1.75	15.12
		450	0.52 ± 0.07	1.99			89.68	10.32	2.74	23.85
EU2–73	1	200	0.53 ± 0.05	0.17	97.48	2.52	96.45	3.55	0.98	26.77
		300	0.52 ± 0.06	0.80			96.71	3.29	1.05	31.11
		450	0.50 ± 0.10	1.89			96.52	3.48	1.78	44.09
	3	200	0.55 ± 0.05	1.69			96.46	3.54	0.52	14.14
		300	0.53 ± 0.07	0.68			97.05	2.95	0.79	26.05
		450	0.52 ± 0.08	1.06			97.26	2.74	0.63	22.66

studied sample, contributing to the robustness of the findings in understanding the compositional characteristics of coated layers.

4. Conclusion

The study presents the CF-LIBS quantification of W—Ta coated layer on a Mo substrate as a primary material for plasma-facing components (PFCs) in fusion devices. The quantification results shows a relative error of 12–40% for W and ~ 2% for Ta when compared with the GDOES results. The study conducted a thorough examination of layer thickness of the samples with varying compositions of WTa-coatings on a Mo substrate using ps-LIBS. And further extended the depth analysis through crater analysis using confocal microscopy providing the details about crater size, depth, and the thickness of the layer. The conventional

GDOES method has been included, providing depth information on layer and revealed significant agreement between the two techniques. Three sets of observation are investigated and among them 300 ns - 300 ns gate width and gate delay is found to be the best suited. An presented spectra highlighting the intensity variations in W I-II and Ta I-II lines within the layer with different laser shots through the sample surface. It is evident that the Mo lines started to appear at the interface of the layer and substrate and becomes prominent as laser pulses go through the sample surface.

The CF-LIBS quantification results reflects higher errors in Ta quantification which is present at low concentration in the sample. Also, deuterium is detected solely in the signal from the first laser shot of ps-LIBS, this majorly affects the depth resolution and quantification of WTaD sample. Therefore, further investigation is required in this area of study. This study is aimed to present a comprehensive analysis of depth profile of WTa coating with ps-LIBS and CF-LIBS, backed up by validating results from GDOES and confocal microscopy scans. The complementary nature of LIBS and GDOES, coupled with the detailed crater analysis, collectively strengthens the credibility and comprehensiveness of the findings in characterizing WTa-coated fusion-relevant materials.

CRediT authorship contribution statement

Shweta Soni: Writing – original draft, Visualization, Methodology, Investigation, Formal analysis. **Sahithya Atikukke:** Writing – review & editing, Visualization, Investigation, Formal analysis. **Matej Veis:** Writing – review & editing, Formal analysis. **Nima Bolouki:** Methodology, Investigation. **Pavol Ďurina:** Methodology, Investigation. **Pavel Dvořák:** Writing – review & editing, Supervision, Resources. **Martina Mrkvičková:** Investigation. **Eduard Grigore:** Resources, Investigation. **Pavel Veis:** Writing – review & editing, Visualization, Supervision, Project administration, Formal analysis, Conceptualization.

Declaration of competing interest

The authors affirm that they do not have any known competing financial interests or personal relationships that could have been perceived to influence the work reported in this paper.

Data availability

Data will be made available on request.

Acknowledgement

This work has been carried out within the framework of the EUROfusion Consortium, funded by the European Union via the Euratom Research and Training Programme (Grant Agreement No 101052200 – EUROfusion). Views and opinions expressed here are however those of the author(s) only and do not necessarily reflect those of the European Union or European Commission. Neither the European Union nor the European Commission can be held responsible for them. The authors acknowledge the Scientific Grant Agency of the Slovak Republic (contract number- VEGA-1/0803/21, VEGA-2/0144/21), the Slovak Research and Development Agency (APVV-16-0612 and APVV-22-0548), and SS acknowledges Grant UK (UK/3139/2024) for financial support. This research has been supported by the Project LM2018097 funded by Ministry of Education, Youth and Sports of the Czech Republic.

References

[1] G. Maurya, A. Roldán, P. Veis, A. Pathak, P. Sen, A review of the LIBS analysis for the plasma-facing components diagnostics, J. Nucl. Mater. 541 (2020) 152417.
[2] A. Roldan, V. Dwivedi, M. Pisarčík, M. Veis, J. Miškovičová, Y. Halahovets, P. Šiffalovic, M. Držík, P. Veis, LIBS investigation of metals suitable for plasma-facing components: characteristics and comparison of picosecond and nanosecond regimes, Fusion Eng. Des. 172 (2021) 112898.
[3] C. Ruset, E. Grigore, H. Maier, R. Neu, H. Greuner, M. Mayer, G. Matthews, Development of W coatings for fusion applications, Fusion Eng. Design 86 (9–11) (2011) 1677–1680.
[4] M. Kaufmann, R. Neu, Tungsten as first wall material in fusion devices, Fusion Eng. Design 82 (5–14) (2007) 521–527.
[5] S. Nogami, I. Ozawa, D. Asami, N. Matsuta, S. Nakabayashi, S. Baumgärtner, L. Philipp, K. Yabuuchi, T. Miyazawa, Y. Kikuchi, et al., Tungsten–tantalum alloys for fusion reactor applications, J. Nucl. Mater. 566 (2022) 153740.
[6] F. Colao, S. Almaviva, L. Caneve, G. Maddaluno, T. Fornal, P. Gasior, M. Kubkowska, M. Rosinski, Libs experiments for quantitative detection of retained fuel, Nucl. Mater. Energy 12 (2017).
[7] H. Van Der Meiden, S. Almaviva, J. Butikova, V. Dwivedi, P. Gasior, W. Gromelski, A. Hakola, X. Jiang, I. Jõgi, J. Karhunen, et al., Monitoring of tritium and impurities in the first wall of fusion devices using a LIBS based diagnostic, Nucl. Fusion 61 (12) (2021) 125001.
[8] G. Maddaluno, S. Almaviva, L. Caneve, F. Colao, V. Lazic, L. Laguardia, P. Gasior, M. Kubkowska, et al., Detection by LIBS of the deuterium retained in the FTU toroidal limiter, Nucl. Mater. Energy 18 (2019) 208–211.
[9] P. Veis, A. Roldán, V. Dwivedi, J. Karhunen, P. Paris, I. Jõgi, C. Porosnicu, C. Lungu, V. Nemanic, A. Hakola, Quantification of H/D content in be/W mixtures coatings by CF-LIBS, Phys. Scr. 2020 (T171) (2020) 014073.
[10] E. Marenkov, I. Tsygvintsev, Y.M. Gasparyan, A. Stepanenko, Assessment of laser induced breakdown spectroscopy accuracy for determination of hydrogen accumulation in tungsten, Nucl. Mater. Energy 28 (2021) 101029.
[11] L. Sun, D. Wu, C. Li, J. Wu, S.-H. Hong, E. Bang, Z. Hu, F. Ding, G. Luo, H. Ding, Characterization of the impurity features deposited on the boronization tungsten tiles exposed in kstar tokamak using laser-induced breakdown spectroscopy, Nucl. Mater. Energy 31 (2022) 101174.
[12] V. Morel, B. Pérès, A. Bultel, A. Hideur, C. Grisolia, Picosecond LIBS diagnostics for tokamak in situ plasma facing materials chemical analysis, Phys. Scr. 2016 (T167) (2016) 014016.
[13] A. Roldán, M. Pisarčík, M. Veis, M. Držík, P. Veis, Calibration-free analysis of a tungsten-based target for diagnostics of relevant fusion materials comparing picosecond and nanosecond LIBS, Spectrochim. Acta B At. Spectrosc. 177 (2021) 106055.
[14] V. Margetic, A. Pakulev, A. Stockhaus, M. Bolshov, K. Niemax, R. Hergenröder, A comparison of nanosecond and femtosecond laser-induced plasma spectroscopy of brass samples, Spectrochim. Acta B At. Spectrosc. 55 (11) (2000) 1771–1785.
[15] K. Eland, D. Stratis, T. Lai, M. Berg, S. Goode, S. Angel, Some comparisons of LIBS measurements using nanosecond and picosecond laser pulses, Appl. Spectrosc. 55 (3) (2001) 279–285.
[16] M. Shirk, P. Molian, A review of ultrashort pulsed laser ablation of materials, J. Laser Appl. 10 (1) (1998) 18–28.
[17] A. Bultel, V. Morel, A. Favre, I. Godard, A. Benyagoub, I. Monnet, A. Sémérok, M. Dinescu, S. Markelj, P. Magaud, et al., Towards ps-LIBS tritium measurements in W/Al materials, Fusion Eng. Design 146 (2019) 1971–1974.
[18] A. Favre, V. Morel, A. Bultel, G. Godard, S. Idlahcen, M. Diez, C. Grisolia, F. Perry, Interface detection by picosecond laser-induced breakdown spectroscopy (LIBS): application to a physical vapor deposited tungsten layer on a copper-chromium-zirconium substrate, Opt. Laser Technol. 150 (2022) 107913.
[19] A. Roldán, V. Dwivedi, M. Veis, S. Atikukke, H. van der Meiden, M. Držík, P. Veis, Quantification of hydrogen isotopes by CF-LIBS in a W-based material (WZr) at atmospheric pressure: from ns towards ps, Phys. Scr. 96 (12) (2021) 124061.
[20] I. Jõgi, J. Ristkok, J. Raud, J. Butikova, K. Mizohata, P. Paris, Laser-induced breakdown spectroscopy for hydrogen detection in molybdenum at atmospheric pressure mixtures of argon and nitrogen, Fusion Eng. Design 179 (2022) 113131.
[21] P. Paris, J. Butikova, M. Laan, A. Hakola, I. Jogi, J. Likonen, E. Grigore, C. Ruset, Comparison of LIBS results on ITER-relevant samples obtained by nanosecond and picosecond lasers, Nucl. Mater. Energy 18 (2019) 1–5.
[22] V. Dwivedi, M. Veis, A. Roldán, E. Grigore, F. Baiasu, I. Radovič, Z. Siketić, P. Veis, CF-LIBS study of pure ta, and WTa+ D coating as fusion-relevant materials: a step towards future in situ compositional quantification at atmospheric pressure, Eur. Phys. J. Plus 136 (11) (2021) 1177.
[23] A. Ciucci, M. Corsi, V. Palleschi, S. Rastelli, A. Salvetti, E. Tognoni, New procedure for quantitative elemental analysis by laser-induced plasma spectroscopy, Appl. Spectrosc. 53 (8) (1999) 960–964.
[24] Z. Hu, D. Zhang, W. Wang, F. Chen, Y. Xu, J. Nie, Y. Chu, L. Guo, A review of calibration-free laser-induced breakdown spectroscopy, TrAC Trends Anal. Chem. 152 (2022) 116618.
[25] C. Ruset, E. Grigore, M. Mayer, F. Baiasu, C. Porosnicu, S. Krat, A. Widdowson, J. Likonen, M. Analytis, R. Meihsner, et al., Deuterium and beryllium depth profiles into the w-coated jet divertor tiles after iter-like wall campaigns, Nucl. Mater. Energy 30 (2022) 101151.
[26] J. Rakovskỳ, J. Krištof, P. Cermák, M. Kociánová, P. Veis, O. Musset, Measurement of echelle spectrometer spectral response in uv, in: J. Safrankova, J. Pavlu (Eds.), WDS'11 Proceedings of Contributed Papers: Part III-Physics, 2011, pp. 257–262. Prague, Matfyzpress.
[27] E. Tognoni, G. Cristoforetti, S. Legnaioli, V. Palleschi, Calibration-free laser-induced breakdown spectroscopy: state of the art, Spectrochim. Acta B At. Spectrosc. 65 (1) (2010) 1–14.
[28] M. Horňáčková, J. Plavčan, J. Rakovskỳ, V. Porubčan, D. Ozdín, P. Veis, Calibration-free laser induced breakdown spectroscopy as an alternative method for found meteorite fragments analysis, Eur. Phys. J.-Appl. Phys. 66 (1) (2014) 10702.

[29] M.A. Gigosos, M.A. Gonzalez, V. Cardenoso, Computer simulated balmer-alpha,-beta and-gamma stark line profiles for non-equilibrium plasmas diagnostics, Spectrochim. Acta B At. Spectrosc. 58 (8) (2003) 1489–1504.
[30] P. Smith, C. Heise, J. Esmond, et al., Atomic spectral line database from CD-ROM 23 of rl kurucz, URL address: http://cfa-www.harvard.edu/amdata/ampdata/kurucz23/sekur.html, 1995 (accessed 20 September 1999).
[31] A. Kramida, Y. Ralchenko, J. Reader, Team 2018, NIST Atomic Spectra Database (version 5.6. 1), Gaithersburg, MD: National Institute of Standards and Technology http://physics. nist. gov/asd (2014).
[32] J. Hermann, C. Gerhard, E. Axente, C. Dutouquet, Comparative investigation of laser ablation plumes in air and argon by analysis of spectral line shapes: insights on calibration-free laser-induced breakdown spectroscopy, Spectrochim. Acta B At. Spectrosc. 100 (2014) 189–196.